

Optimizing Multiple-Flyby Orbits for Increasing the Resolution of Space Telescopes

Dmitry M. Pisarevsky* and Pini Gurfil†

Technion—Israel Institute of Technology, Haifa 32000, Israel

DOI: 10.2514/1.39925

This paper investigates trajectories for spaceborne observatories with long times of flight high above the ecliptic plane. A large normal displacement is necessary for mitigating the effect of noise generated by the interplanetary (zodiacal) dust cloud, thus increasing resolution and reducing the sizes of the telescopes. Flyby paths using multiple-gravity-assist maneuvers near Earth and Venus are used to reach Jupiter, where the inclination is increased and the final orbit is produced. The trajectory design is performed using a memetic algorithm, which is a combination of global and local optimizers. The global search for optimal trajectories with minimal energy requirements and short transfer times to the highly inclined destination orbit is performed using a niching genetic algorithm improved by a gradient-based local optimization. The optimization yielded three candidate paths, each accompanied by, at most, one deep-space maneuver. The resulting energy-efficient orbits are characterized by large displacements normal to the ecliptic plane, thereby providing prolonged observation times in the interplanetary-dust-noise-free celestial sphere.

Nomenclature

a	=	semimajor axis, km
e	=	eccentricity
f	=	true anomaly, rad
h_{fb}	=	flyby altitude, km
h_m	=	minimal allowed flyby altitude, km
i	=	inclination, rad
p	=	semilatus rectum, km
R_{pl}	=	equatorial radius of the flyby planet, km
r	=	orbital radius of the spacecraft, km
r_{pl}	=	orbital radius of the planet, km
\mathbf{V}	=	spacecraft heliocentric velocity vector, km/s
\mathbf{V}_{pl}	=	planet heliocentric velocity vector, km/s
$V_{pl,r}$	=	planet radial velocity, km/s
$V_{pl,\theta}$	=	planet transverse velocity, km/s
V_r	=	spacecraft radial velocity, km/s
V_θ	=	spacecraft transverse velocity, km/s
\mathbf{V}_∞	=	spacecraft hyperbolic excess velocity vector, km/s
$\mathbf{V}_{\infty/J}$	=	spacecraft hyperbolic excess velocity vector relative to Jupiter, km/s
$\mathbf{V}_{\infty/\oplus}$	=	spacecraft hyperbolic excess velocity vector relative to Earth, km/s
μ_{pl}	=	gravitational parameter of the flyby planet, km ³ /s ²
μ_\odot	=	gravitational parameter of the sun, km ³ /s ²

Subscript

0 = initial value

Superscripts

+ = after flyby
 – = before flyby

I. Introduction

ONE of the endeavors of NASA and ESA is understanding the origin, evolution, and future of life in the universe. Spaceborne observation missions such as Kepler, Darwin, James Web Space Telescope, and Terrestrial Planet Finder (TPF) will play a significant role in these studies.[‡]

The stringent optical resolution of the aforementioned missions requires a judicious orbital design. Usually, three main alternatives are considered: heliocentric Earth-trailing orbits, heliocentric Earth drift-away orbits, and halo/Lissajous orbits about the sun–Earth L₂ libration point. Although these orbits satisfy most of the programmatic constraints of space observation missions, they may limit the maximal imaging resolution. This is because these orbits lie very close to the ecliptic plane, in which the brightness of the zodiacal dust cloud is maximal. This interplanetary dust (IPD) forms a pancake-shaped cloud in the solar system. The typical diameter of a dust particle is ~10 μm. It is composed of silicates, ices, and other minerals.

The IPD has a potentially serious impact on the ability of spaceborne observatories to detect and study their targets. Reference [1] shows that for a 1 AU (astronomical unit) TPF interferometer mission, the local zodiacal background constitutes roughly 70% of the total noise. However, the intensity of the IPD brightness is reduced when moving in a direction normal to the ecliptic plane. At 0.2 AU above the ecliptic plane, roughly 50% of the normalized brightness is avoided, and at 0.3 AU above the ecliptic plane, about 70% of the brightness is truncated. Thus, the region in which the normal displacement is above 0.3 AU or below –0.3 AU will be referred to as the *observable region*; the *tarnished region* is where the normal excursion is smaller than 0.3 AU. Consequently, the time intervals spent in these regions are referred to as the *observable time* and the *tarnished time*, respectively.

The fact that the IPD brightness extinguishes while ascending above the ecliptic plane leads to the idea of constructing new orbits for spaceborne observatories, orbits that are highly inclined, with considerable out-of-ecliptic displacements. However, although higher excursions reduce the noise generated by the IPD emission, the energetic requirements involved may be substantial. For example, [2,3] presented three types of out-of-ecliptic, non-Keplerian orbits obtained by applying genetic-algorithm-based optimization on the restricted three-body problem (R3BP) model. These orbits resulted in a significantly reduced background noise

Received 21 July 2008; revision received 2 February 2009; accepted for publication 5 February 2009. Copyright © 2009 by the authors. Published by the American Institute of Aeronautics and Astronautics, Inc., with permission. Copies of this paper may be made for personal or internal use, on condition that the copier pay the \$10.00 per-copy fee to the Copyright Clearance Center, Inc., 222 Rosewood Drive, Danvers, MA 01923; include the code 0022-4650/09 \$10.00 in correspondence with the CCC.

*Research Staff Member, Faculty of Aerospace Engineering; aedmitry@technion.ac.il.

†Senior Lecturer, Faculty of Aerospace Engineering; pgurfil@technion.ac.il. Associate Fellow AIAA.

[‡]Data available online at <http://origins.jpl.nasa.gov/index1.html> [retrieved 1 July 2008].

from the IPD radiation compared with a 1 AU in-plane orbit. However, the two operational orbits presented in [3] required considerable energy. The first orbit required energy that is equivalent to half the energy for a direct trip to Jupiter (without gravity assists), and the other required twice that energy. The maximal displacements of these orbits above the ecliptic were, respectively, 0.22 and 0.37 AU.

Another example of a highly inclined orbit is the Ulysses spacecraft trajectory.[§] Ulysses is aimed at the exploration of the sun's polar environment. Because direct injection from Earth into a solar polar orbit is infeasible, a powerful gravity assist is required to achieve a high-inclination orbit. As a result, Ulysses was launched with a high speed toward Jupiter in October 1990. Following the flyby of Jupiter in February 1992, the spacecraft was redirected to a highly inclined heliocentric orbit. The achieved inclination was roughly 80 deg relative to the ecliptic plane, which established a maximal normal displacement of 2.68 AU.

In the aforementioned approaches, high energy consumption was needed to reach a high-inclination orbit with a long observation time. In the first approach, the solutions were obtained by examining the spatial R3BP; higher inclinations resulted in higher Jacobi constants [4], requiring considerable thrust. In the second approach, a gravity-assisted maneuver near Jupiter was used to reach a high inclination. However, to use the latter strategy, the energy at launch has to be sufficiently large. This stems from two reasons: First, much energy is required for a direct Earth–Jupiter transfer. Second, to obtain highly inclined orbits, the total energy has to be much higher than the energy of the Hohmann transfer (assuming circular coplanar orbits of Earth and Jupiter).

This paper proposes an alternative energy-efficient orbit design of highly inclined orbits, which is particularly suitable for spaceborne observatories with typical mission lifetimes of 20 years. The proposed orbits consist of two legs: *acceleration* and *final*. The acceleration leg comprises a series of near-ecliptic interplanetary trajectories patched by gravity-assisted maneuvers near the planets. The final leg consists of a gravity-assisted maneuver near Jupiter, forming the final, highly inclined, heliocentric orbit with maximized observation time. The spacecraft is launched from Earth with a relatively small energy, much lower than the energy of a Hohmann transfer to Jupiter, but still sufficiently large to reach one of the nearest planets and perform the first gravity-assisted maneuver. During each of the interplanetary transfers, if required, a single deep-space maneuver (DSM) is performed to ensure planetary flyby. In some cases, the DSM can be replaced by an auxiliary flyby maneuver (AFM), which is a small impulsive maneuver carried out during a gravity-assisted maneuver to increase the effect of the flyby.

There are many previously published works dedicated to the Earth–Jupiter multiple-gravity-assist transfers (see [5–7] and references therein). In all of these works, the criteria for designing the transfer orbits were 1) the fuel consumption ΔV , including the launch impulse and midway impulses, 2) the time of flight (TOF), and 3) the hyperbolic excess velocity relative to Jupiter, which has to vanish for capture. The current work also uses the first two criteria; however, the third constraint is not imposed, because the final orbit is not a Jovian one.

Obviously, simultaneous minimization of the TOF and the total ΔV is impossible. This leads to a creation of a Pareto front in the search space, representing families of optimal solutions with different weightings of the multiple objectives [8]. One way to perform the global multi-objective optimization is to use niching methods [9]. Instead of converging to a single optimum, niching allows for a number of optimal solutions to coexist and lets the designer choose the appropriate one.

In this paper, we perform a structured stochastic search for a set of parameters (magnitude and direction of the initial hyperbolic excess velocity relative to Earth, the flyby altitudes above planets, and a binary parameter indicating the type of the first interplanetary transfer) that minimize the total ΔV required for the Earth–Jupiter multiple-gravity-assist transfer. The search is performed using a

memetic algorithm (MA) [10], which is a niching genetic algorithm (GA) [11,12] combined with a local optimizer. Using MA instead of GA can dramatically reduce the search time. From the resulting candidate optimal solutions, trajectories with low TOFs and high final energy are chosen.

The optimal trajectories designed in this work are characterized by maximized, yet approximately equal, observation times below and above 0.3 AU relative to the ecliptic plane, which enables imaging of objects both in the north and south celestial spheres. These orbits cannot be obtained by simply reaching the maximal possible inclination after the Jupiter flyby; although a maximal heliocentric inclination would lead to the maximal *total* observation time, it will generally not provide equal observation times below and above the ecliptic during a limited-time mission.

II. Problem Formulation

A. Approach

We consider orbits with multiple-gravity-assist maneuvers in a system comprising the sun (m_1), the flyby planet (m_2), and the spacecraft (m_3), all considered as point masses governed by Newton's gravitational law. In practice, the influence of m_3 on the motion of the other bodies can be neglected, $m_3 = 0$, which implies that the planet follows a Keplerian orbit about the sun. If this orbit is circular, the resulting setup is called the circular R3BP. The canonical scaling of time, length, and mass units [4] uses the planet's orbital radius and the inverse of the angular velocity as the length and time units, respectively, and uses $m_1 + m_2$ as the mass unit. The only remaining parameter is $\mu \triangleq m_2/(m_1 + m_2)$. The circular R3BP may be further simplified when $\mu \ll 1$. In this case, the heliocentric spacecraft orbit is nearly Keplerian everywhere, except for a narrow vicinity of the planet, in which the spacecraft experiences a short impulse of gravitational attraction. When $\mu \rightarrow 0$ simultaneously with the flyby distance, the impulse duration tends to zero, and the resulting trajectory is similar to an ideal elastic collision. This asymptotic case is called, after Poincaré [13], the *problem of trajectories with consecutive collisions* (an alternative name is *zero-point patched conic model*). It deals with a chain of collisional trajectories (i.e., Keplerian arcs with collisions at one or both ends).

The geometry of this problem is depicted by Fig. 1. In this figure, \mathbf{V}_{pl} and \mathbf{V} are the heliocentric velocities of the planet and the spacecraft, respectively; δ is the turning angle of the hyperbolic excess velocity vector; and \mathbf{V}_∞ is the velocity of the spacecraft relative to the planet. Letting the superscripts – and + denote before and after flyby, respectively, we can write

$$\|\mathbf{V}_\infty^-\| = \|\mathbf{V}_\infty^+\| = V_\infty \quad (1)$$

In the collision model setup, a multiple-gravity-assist interplanetary transfer consists of *segments*, in which each segment is patched to the following one by a gravity-assisted maneuver. In the case of an *unpowered segment*, the transfer is ballistic, and the spacecraft flies

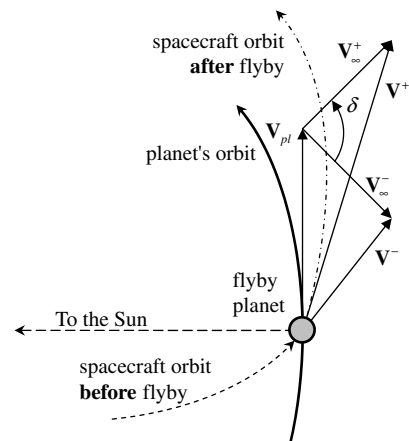


Fig. 1 Asymptotic case of the flyby: a collision model.

[§]Data available online at <http://ulysses.jpl.nasa.gov> [retrieved 1 July 2008].

on a Keplerian arc; in the case of a *powered segment*, the transfer consists of several Keplerian arcs patched by DSMs. The arcs before and after each of the flybys must obey the following *concatenation rules*: 1) preservation of relative velocity with respect to the flyby planet, 2) feasible flyby altitude, and 3) synchronization, meaning that at the end of the arc, the spacecraft has to encounter the flyby planet.

B. Concatenation Rules

The first concatenation rule for a circular planet orbit was first described by Tisserand, as detailed by Szebehely [4] (alternatively, this rule can be obtained from the preservation of Jacobi's constant in the circular R3BP). It reads

$$-\frac{V_\infty^2}{\mu_\odot} + \frac{3}{r_{\text{pl}}} = 2\sqrt{\frac{p}{r_{\text{pl}}^3}} \cos i + \frac{1}{a} \quad (2)$$

where r_{pl} is the orbital radius of the planet, μ_\odot is the gravitational parameter of the sun, a is the semimajor axis, and p is the semilatus rectum. Based on the relationship (1), Eq. (2) leads to the following connection between the orbital elements of the spacecraft before and after the flyby:

$$2\sqrt{\frac{p^-}{r_{\text{pl}}^3}} \cos i^- + \frac{1}{a^-} = 2\sqrt{\frac{p^+}{r_{\text{pl}}^3}} \cos i^+ + \frac{1}{a^+} \quad (3)$$

If the planet's orbit is elliptic, Tisserand's criterion can be rewritten in terms of the radial and transverse velocities of the spacecraft, denoted by V_r and V_θ , respectively, and the radial and transverse velocities of the planet, $V_{\text{pl},r}$ and $V_{\text{pl},\theta}$, respectively, as seen in Fig. 2. The expressions for these velocities are

$$V_r = e \sin f \sqrt{\frac{\mu}{a(1-e^2)}}, \quad V_\theta = \frac{\sqrt{\mu a(1-e^2)}}{r} \quad (4)$$

where f is the true anomaly, and r is the orbital radius, given by

$$r = \frac{a(1-e^2)}{1+e \cos f} \quad (5)$$

The modified criterion, obtained in [14], is given by

$$V_\infty^2 = (V_r - V_{\text{pl},r})^2 + V_\theta^2 + V_{\text{pl},\theta}^2 - 2V_\theta V_{\text{pl},\theta} \cos i \quad (6)$$

The second concatenation rule requires that the flyby altitude (the minimal distance to the planet during a hyperbolic flyby) be above some allowed threshold. The flyby altitude given an elliptic planetary orbit can be written as [14]

$$h_{\text{fb}} = \frac{\mu_{\text{pl}}}{V_\infty^2} \left[\sqrt{\frac{2V_\infty^2}{\sqrt{\Delta V_r^2 + \Delta V_\theta^2 + 4V_\theta V_{\text{pl},\theta} \sin^2(\Delta i/2)}}} - 1 \right] - R_{\text{pl}} \quad (7)$$

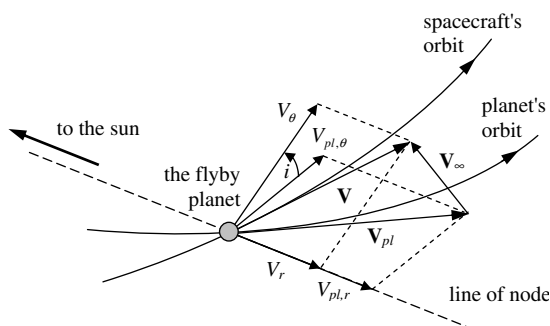


Fig. 2 Velocity diagram corresponding to the flyby moment, with the inclination of the spacecraft's orbit, i , measured relative to the planet's orbit.

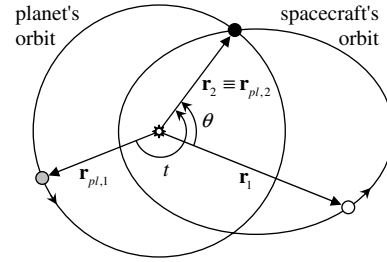


Fig. 3 Geometric representation of the synchronization condition.

where h_{fb} is the flyby altitude, μ_{pl} and R_{pl} are the gravitational parameter and the equatorial radius of the flyby planet, respectively, and

$$\Delta V_r \triangleq V_r^+ - V_r^-, \quad \Delta V_\theta \triangleq V_\theta^+ - V_\theta^-, \quad \Delta i \triangleq i^+ - i^- \quad (8)$$

Therefore, two arcs [before and after the flyby (see Fig. 1)] can be patched if $h_{\text{fb}} > h_m$, where h_m is the minimal allowed flyby altitude above the planet.

The third concatenation rule, the synchronization condition, establishes a coupling between the angular size of an arc and the respective flight time. According to Lambert's theorem [15], the flight time over an arc is

$$t = \sqrt{a^3/\mu_\odot} [(\alpha - \sin \alpha) - (\beta - \sin \beta)] \quad (9)$$

The variables α and β are defined by

$$r_1 + r_2 + c = 4a \sin^2(\alpha/2) \quad (10)$$

$$r_1 + r_2 - c = 4a \sin^2(\beta/2) \quad (11)$$

and

$$c \triangleq |\mathbf{r}_2 - \mathbf{r}_1| = \sqrt{r_1^2 + r_2^2 - 2r_1 r_2 \cos \theta} \quad (12)$$

The vectors \mathbf{r}_1 and \mathbf{r}_2 are the initial and final position vectors for the arc, $r_1 = \|\mathbf{r}_1\|$, $r_2 = \|\mathbf{r}_2\|$, and θ is the transfer angle of the arc, as shown in Fig. 3.

The procedure of obtaining the arc parameters guaranteeing an encounter between the spacecraft and flyby planet is as follows. For a given initial position of the spacecraft, \mathbf{r}_1 (see Fig. 3), the position of the next flyby planet, $\mathbf{r}_{\text{pl},1}$, and the time until the encounter, t , calculate the final position vector, $\mathbf{r}_2 \equiv \mathbf{r}_{\text{pl},2}$, using the known orbital parameters of the planet. Then, from \mathbf{r}_1 and \mathbf{r}_2 , calculate the transfer angle θ using Eq. (12). Finally, using Eqs. (10) and (11), calculate all the remaining transfer parameters.

III. Optimal Solutions

In this section, we discuss the methodology used for trajectory optimization of spaceborne observation missions and describe the general approach, optimization method, objective function, and constraints. We use the following simplified model of the solar system. All planets orbit the sun in the ecliptic plane; Earth and Venus follow circular orbits, and Mars and Jupiter follow eccentric orbits. The approximate planetary positions were calculated using a simplified Jet Propulsion Laboratory model,⁶ where the inclination of the planets is zero.

A. Approach

As mentioned previously, the mission consists of two legs: acceleration and final. The TOF on these legs is defined by t_1 and t_2 , respectively. We write $t_2 = t_{\text{obs}} + t_{\text{tar}}$, where t_{obs} is the total observation time, and t_{tar} is the time spent inside the tarnished region.

⁶Available online at http://ssd.jpl.nasa.gov/txt/aprx_pos_planets.pdf [retrieved 1 July 2008].

The total observation times above and below the ecliptic plane are denoted by t_{obs}^+ and t_{obs}^- , respectively, so that $t_{\text{obs}} = t_{\text{obs}}^+ + t_{\text{obs}}^-$. In addition, the total impulsive maneuver during the mission is defined as ΔV . Its value consists of the initial impulsive maneuver ΔV_0 and all the midway DSMs ΔV_{DSM} and AFMs ΔV_{AFM} : that is,

$$\Delta V = \Delta V_0 + \Delta V_{\text{DSM}} + \Delta V_{\text{AFM}} \quad (13)$$

The initial impulsive maneuver ΔV_0 injects the spacecraft into a heliocentric orbit starting from an initial geocentric 200 km circular parking orbit (cf. [15]).

The trajectory design process is divided into two steps, one for each leg. Using the notation presented previously, the acceleration leg should be optimized for a minimal ΔV and a minimal t_1 . We do not attempt to optimize both criteria simultaneously, but instead apply a niching method [9] to find a set of appropriate trajectories with a minimal ΔV . From this set, the trajectory with the minimal t_1 is chosen. Minimization of t_1 is desirable because the mission lifetime is limited to 20 years: that is,

$$t_1 + t_{\text{obs}} + t_{\text{tar}} = 20 \text{ years} \quad (14)$$

Therefore, minimizing t_1 will maximize the TOF of the final leg, $t_{\text{obs}} + t_{\text{tar}}$. The final leg is then optimized to obtain a maximal t_{obs} .

Many numerical methods have been applied to space trajectory optimization problems. Most of these methods used the gradient of the cost function. This approach is suitable for the optimization of the final leg, but is less useful for the acceleration leg, comprising multiple-gravity-assist trajectories. This is because gradient-based optimization is very sensitive to initial guesses; that is, a poor initial guess may converge onto an infeasible solution or onto a local optimum, which can be far from the global optimum. On the other hand, structured stochastic global optimization methods, such as a GA [11], can progress through multiple local optima toward the global optimum. Niching methods such as deterministic crowding [9] enable identification of multiple optima in a given problem and are hence suitable for multi-objective optimization problems similar to the problem at hand.

Yet, GAs are not well suited for fine-tuning of optimal solutions [11]. This can be remedied by incorporating local operators into the recombination step of the GA. This approach gives rise to MAs [10], which are evolutionary algorithms that apply a separate local search process to refine individuals (i.e., improve their fitness). The resulting trajectory optimization methodology is then as follows:

- 1) Trajectories for the acceleration leg are optimized using MAs.
- 2) The trajectory for the final leg, after the Jupiter flyby, is optimized using a gradient-based method.

The optimized degree of freedom in the second step is the direction of $\mathbf{V}_{\infty/J}$, the hyperbolic excess velocity vector relative to Jupiter.

The optimization is split into two parts, due to the obvious fact that trajectories with a higher $\mathbf{V}_{\infty/J}$ will provide longer observation times. To save CPU-consuming calculations at the first leg, we split the process into two legs, thereby optimizing the observation time at the second leg only for good candidate solutions obtained during the first leg.

B. Memetic Algorithms

MAs [10] represent one of the recent areas of research in evolutionary computation. The term MA refers to a combination of an evolutionary (or any population-based approach) search with separate individual learning (i.e., local refinement operators). This procedure yields an optimization methodology that balances the generality of global optimization and the domain-specific functionality of a local search. In this paper, we use a GA enhanced with a deterministic crowding [9] niching mechanism to promote diversity of solutions.

The deterministic crowding algorithm used herein is summarized by the pseudocode described in Fig. 4. The basic premise of the algorithm is that pairs of individuals are recombined to create an offspring. These offspring then replace their closest parent if they are of greater fitness. Deterministic crowding uses a distance measure to determine similarity between individuals. Additionally, deterministic crowding is an elitist niching method. This means that once a peak is discovered, it is never lost from the population.

C. Global Optimization Procedure

1. Parameters

The MA starts from an initial population that can be either supplied by the user or determined randomly. Additional parameters are the population size N (in case the initial population was not supplied), maximal number of generations N_G , and crossover and mutation probabilities, denoted by p_c and p_m , respectively. Crossover is used to create new solution strings from existing strings. Mutation is an occasional random alteration of some value in a given position along the string.

Each run of the MA produces a set of trajectories for a given path. A *path* is a string that indicates the ordered flyby planets. For example, the path EVEEJ indicates a trajectory that starts from Earth, continues to Venus, goes back to Earth, and then, after a heliocentric motion, encounters Earth again before reaching Jupiter. Thus, a path constitutes an additional optimization parameter (it is chosen manually in our experiments). The paths examined were EVEJ, EVEEJ, and EVVEJ. Other paths, including Mars (M) flybys, did not yield notable results (these include EVEVJ, EVMVMJ, EVVVJ, EVEEMJ, EVEVEJ, and EVMVEJ).

```

input : A population of individuals of size  $N$ 
output : The same population with reproduced individuals

1 Shuffle population;
2 for  $i \leftarrow 1$  to  $(N - 1)$  step 2 do
3    $p_1 \leftarrow \text{population}[i]$ ;
4    $p_2 \leftarrow \text{population}[i + 1]$ ;
5    $(c_1, c_2) \leftarrow \text{reproduce}(p_1, p_2)$ ;
6   if [  $\text{distance}(p_1, c_1) + \text{distance}(p_2, c_2)$  ]  $\leq$  [  $\text{distance}(p_1, c_2) + \text{distance}(p_2, c_1)$  ]
7     then
8       if  $\text{fitness}(c_1) > \text{fitness}(p_1)$  then  $p_1 \leftarrow c_1$ ;
9       if  $\text{fitness}(c_2) > \text{fitness}(p_2)$  then  $p_2 \leftarrow c_2$ ;
10    else
11      if  $\text{fitness}(c_2) > \text{fitness}(p_1)$  then  $p_1 \leftarrow c_2$ ;
12      if  $\text{fitness}(c_1) > \text{fitness}(p_2)$  then  $p_2 \leftarrow c_1$ ;
13    end
14 end
15 return population;

```

Fig. 4 Pseudocode describing the deterministic crowding genetic algorithm.

2. Controls and Constraints

The controls are the magnitude and direction of $(\mathbf{V}_{\infty/\oplus})_0$ (the initial hyperbolic excess velocity relative to Earth), which determine the initial spacecraft trajectory; flyby altitudes, which determine the trajectories after each flyby; and a binary parameter ε , which indicates the type of first interplanetary transfer, determined as follows. The initial orbit of the spacecraft crosses Venus's orbit twice; the variable ε indicates which of the crossing points is chosen as the end point of the first interplanetary leg.

In the simplified celestial model used herein, Earth's and Venus's orbits are assumed to be coplanar and circular; therefore, for a given initial spacecraft orbit, the transfer time of the first (Earth–Venus) interplanetary transfer (the time elapsed from launch until crossing Venus's orbit) would set the initial Earth–Venus relative angle. Because this angle repeats every Earth–Venus synodic year, the appropriate launch dates can be calculated. The index set of these dates, constrained to lie between the years 2010 and 2030, is $\{k = 1, 2, \dots\}$, and the corresponding total velocity correction is ΔV_k . A launch date is chosen to minimize the total ΔV .

3. Fitness Function

The global optimization with the parameters and controls defined previously is aimed at finding an optimal solution of the form

$$\Delta V^* = \arg \min_k \Delta V_k = \arg \min_k (\Delta V_0 + \Delta V_{\text{DSM}} + \Delta V_{\text{AFM}})_k \quad (15)$$

D. Local Optimization Procedure

During each interplanetary transfer one impulsive maneuver, at most, is allowed. If j indicates the number of the interplanetary leg, then the j th maneuver's magnitude is $\Delta V_{\text{DSM},j}$ and its direction is $\gamma_{\text{DSM},j}$. The transfer trajectory from planet P_1 to planet P_2 is denoted by $P_1 P_2$. The transfer time from P_1 to the impulse application point P is t_{1P} , and the transfer time from P to P_2 is t_{P2} . The objective function for the local optimization is then

$$f_j(\mathbf{x}) = \Delta V_{\text{DSM},j} \quad (16)$$

where $\mathbf{x} = [t_{1P}, t_{P2}]$; the goal is to find

$$\mathbf{x}^* = \arg \min_{\mathbf{x} \in [0, t_{\text{max}}]} f_j(\mathbf{x}) \quad (17)$$

input	: \mathbf{r}_1 and \mathbf{V}_1	% initial spacecraft's position and velocity vectors
	$\mathbf{r}_{P_2,1}$ and $\mathbf{V}_{P_2,1}$	% initial position and velocity vectors of planet P_2
controllers	: t_{1P} and t_{P2}	
output	: $\Delta V_{\text{DSM},j}$	
1	$[\mathbf{r}_p, \mathbf{V}_p^-] = \text{in_val_pr}(\mathbf{r}_1, \mathbf{V}_1, t_{1P})$	% solving initial value problem. Results are % position and velocity (before the impulse % is applied) vectors at point P.
2	$\mathbf{r}_{P_2,2} = \text{in_val_pr}(\mathbf{r}_{P_2,1}, \mathbf{V}_{P_2,1}, t_{1P} + t_{P2})$	% solving an initial value problem for planet P_2 .
3	$\mathbf{r}_2 \leftarrow \mathbf{r}_{P_2,2}$	% After time $t_{1P} + t_{P2}$ the spacecraft and the % P_2 positions are matched, therefore $\mathbf{r}_2 \equiv \mathbf{r}_{P_2,2}$.
4	$[\mathbf{V}_p^+, \mathbf{V}_2] = \text{lambert_pr}(\mathbf{r}_p, \mathbf{r}_2, t_{P2})$	% solving a boundary value problem (Lambert's % problem). Results are velocity vector % immediately after the impulse and % the heliocentric velocity vector at % P_2 encounter.
5	$\Delta V_{\text{DSM},j} = \ \mathbf{V}_p^+ - \mathbf{V}_p^-\ $	
6	return $\Delta V_{\text{DSM},j}$	

Fig. 5 Pseudocode for the objective function $f_j(\mathbf{x}) = \Delta V_{\text{DSM},j}$.

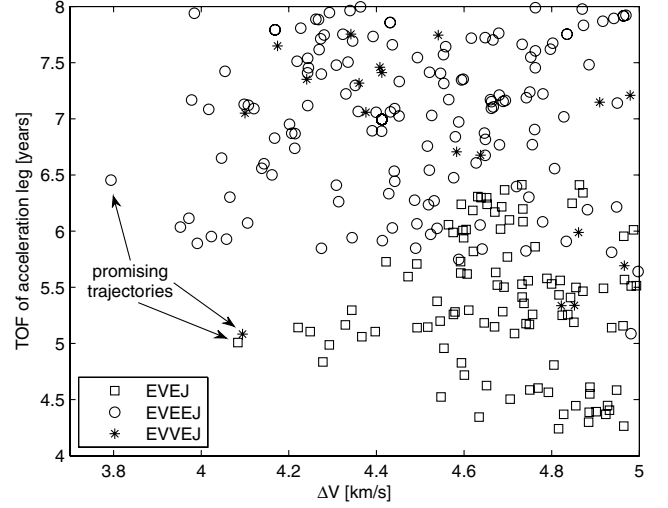


Fig. 6 Memetic algorithm optimization results for EVEJ, EVEEJ, and EVVEJ transfers.

where t_{max} , the upper bound on the transfer times, was set to 1 year. If the impulse is applied in a close vicinity of P_1 ($t_{1P}^* \approx 0$) or P_2 ($t_{P2}^* \approx 0$), then the impulse is considered as an AFM, so that

$$f_j(\mathbf{x}) = \Delta V_{\text{AFM},j} \quad (18)$$

The pseudocode of the function $f_j(\mathbf{x})$ is presented in Fig. 5. This local optimization can be carried out using any gradient-based algorithm. We used the MATLAB function `fminsearch`.

IV. Results

This section presents simulation results for the Earth–Jupiter multiple-gravity-assist trajectories obtained via the MA and the final observation orbits.

A. Multiple-Gravity-Assist Trajectories of the Acceleration Leg

The parameter values for all runs were as follows:

$$N = 300, \quad N_G = 500, \quad p_c = 0.95, \quad p_m = 0.05 \quad (19)$$

Launch dates were constrained between the years 2010 and 2030. The initial hyperbolic excess velocity relative to Earth satisfied

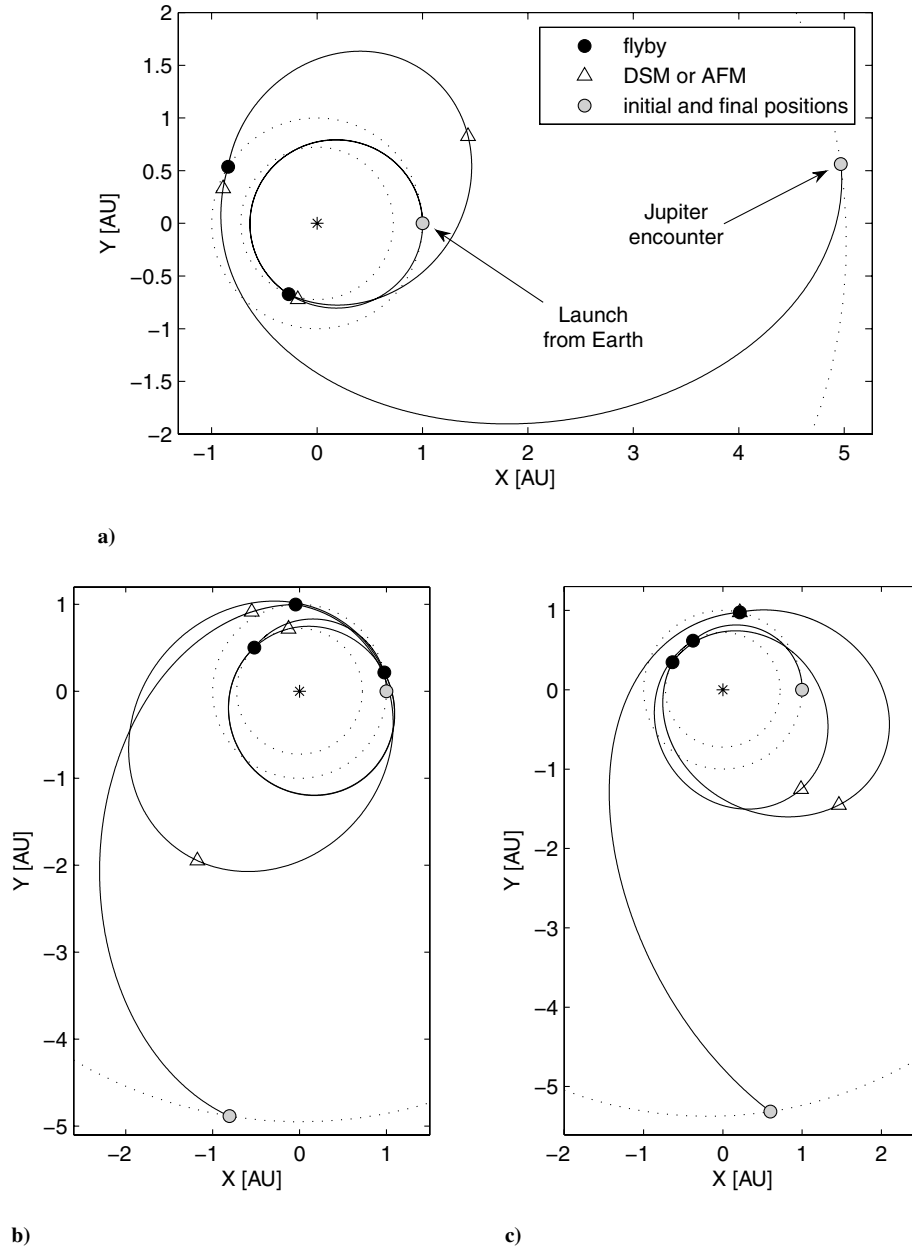


Fig. 7 Chosen optimal trajectories: a) EVEJ, b) EVEEJ, and c) EVVEJ.

Table 1 Characteristics of the chosen optimal trajectories of the acceleration leg

Path	Solutions		
	EVEJ ^c	EVEEJ	EVVEJ
Launch date	4 Dec. 2016	23 Apr. 2028	4 Dec. 2013
$(V_{\infty/\oplus})_0$ initial hyperbolic excess velocity relative to Earth, km/s	3.53	2.85	3.19
$V_{\infty/J}$ hyperbolic excess velocity relative to Jupiter, km/s	6.21	6.32	9.14
Impulsive maneuvers ^{a,b} : ΔV_0 , $\Delta V_{\text{DSM},j}$ or $\Delta V_{\text{AFM},j}$, km/s	3.78, 0.024, 0.014, 0.27	3.59, 0.024, 0.111, 0.072	3.68, 0.241, 0.158, 0.019 ^b
Times ^a (from launch) of the $\Delta V_{\text{DSM},j}$ or $\Delta V_{\text{AFM},j}$ and flybys, days	173, 440, 610, 880, 890, 1829	118, 453, 743, 1190, 1555, 1578, 2357	108, 351, 576, 809, 1175, 1175 ^b , 1857
h_{fb} flyby altitudes, km	1030, 310	350, 3750, 370	330, 340, 340
Total TOF, years	5.01	6.45	5.08
Total ΔV , km/s	4.08	3.8	4.09

^aPresented in order of their appearance.

^bThe AFM.

^cFirst interplanetary leg with a DSM.

Table 2 Orbits of the final leg

Path	a , AU	e	i , deg	Observation times t_{obs}^+/t_{obs}^- , years	Flyby heights near Jupiter, 10^6 km
EVEJ	6.29	0.21	25	7/7	1.4
EVVEJ	5.76	0.14	26	6.4/6.4	1.6
EVVEJ	6.29	0.15	40	7.2/7.2	0.75

$$2.5 \text{ km/s} \leq V_{\infty/\oplus} \leq 4.5 \text{ km/s} \quad (20)$$

The direction of $V_{\infty/\oplus}$, measured counterclockwise relative to the initial position vector, was bounded between $\pi/2$ and $3/2\pi$ to provide negative initial radial velocity; for all the flyby altitudes, $h_{fb} \geq 300$ km. If an impulsive maneuver was applied during the first interplanetary leg, additional constraints were added: the magnitude of the maneuver must not exceed 1 km/s, and the time until impulse application must not exceed 1 year.

To obtain the feasible trajectories for the acceleration leg, several paths were tested. The most promising paths were EVEJ, EVVEJ, and EVVEJ. Figure 6 depicts the TOF and the total ΔV obtained by the MA. From these results, three promising trajectories with low ΔV and TOF were chosen (see the annotation on Fig. 6).

The chosen trajectories are shown in Fig. 7. The launch position and the position of the final encounter with Jupiter are marked by gray circles. The positions of all the gravity-assisted maneuvers are shown as black circles. The DSMs and AFMs are represented by triangles. The dotted lines depict the orbits of Venus (the inner circle), Earth (the middle circle), and Jupiter (the outer circle).

The main characteristics of the chosen trajectories are presented in Table 1. The EVEJ and EVVEJ trajectories have a relatively short TOF and small ΔV ; however, the first trajectory arrives at Jupiter with low V_{∞} . This would result in a relatively low-inclination orbit in the final leg. As opposed to this, the EVVEJ trajectory arrives at Jupiter with a much higher V_{∞} . Therefore, it can produce a highly inclined orbit that will be well suited to spaceborne observatories. The EVVEJ trajectory has a long TOF, but the ΔV is the smallest of all trajectories. This trajectory has low Jupiter-arrival velocity, similar to the EVEJ trajectory.

Note that in the EVEJ trajectory, a DSM is applied during the first interplanetary leg, whereas all the other trajectories do not require a DSM. Finally, during the EVVEJ trajectory, an AFM impulse is given during the last Earth flyby.

B. Observation Orbits of the Final Leg

This section discusses the final leg of the spaceborne observation mission: the leg on which observation data are collected and transmitted to Earth. The goal is to find an orbit with maximal observation time t_{obs} , according to the following constraints:

- 1) The mission lifetime is 20 years.
- 2) The observation times below and above the ecliptic plane are roughly the same (i.e., $t_{obs}^+ \approx t_{obs}^-$).
- 3) Perihelion of the final orbit has to be above Mercury's orbit. This to avoid both large thermal shielding and optical detector saturation.

The final orbit is a continuation of the acceleration leg trajectory after Jupiter flyby. Therefore, the promising trajectories, found in the previous section, will serve as initial conditions for the final-leg trajectory. The parameters of the orbits before and after the flyby are connected by the relationship described in Eq. (3). Using this constraint, the final orbit is unambiguously defined for a given V_{∞} and two additional parameters of the orbit (e.g., V_r and V_{θ}). The velocity V_{∞} can be obtained from the last arc of the acceleration leg. Therefore, the only controllers for the t_{obs} optimization are V_r and V_{θ} or some equivalents, implying that the optimization can be performed using a gradient-based algorithm (e.g., MATLAB's `fminsearch`).

Table 2 presents results for the final orbits with maximal t_{obs} . Each of the orbits results from the gravity-assisted maneuver near Jupiter performed at the end of the acceleration leg obtained in the previous section. For convenience, the final orbits (and hence the complete

mission trajectories) inherit their names from the acceleration leg's trajectories. Figure 8 presents these orbits along with the acceleration leg's trajectories. The dotted circles again depict the orbits of Venus, Earth, and Jupiter. Figure 9 shows the heights (relative to the ecliptic plane) of the spacecraft during the mission lifetime. The dotted lines separate the tarnished region from the observable region.

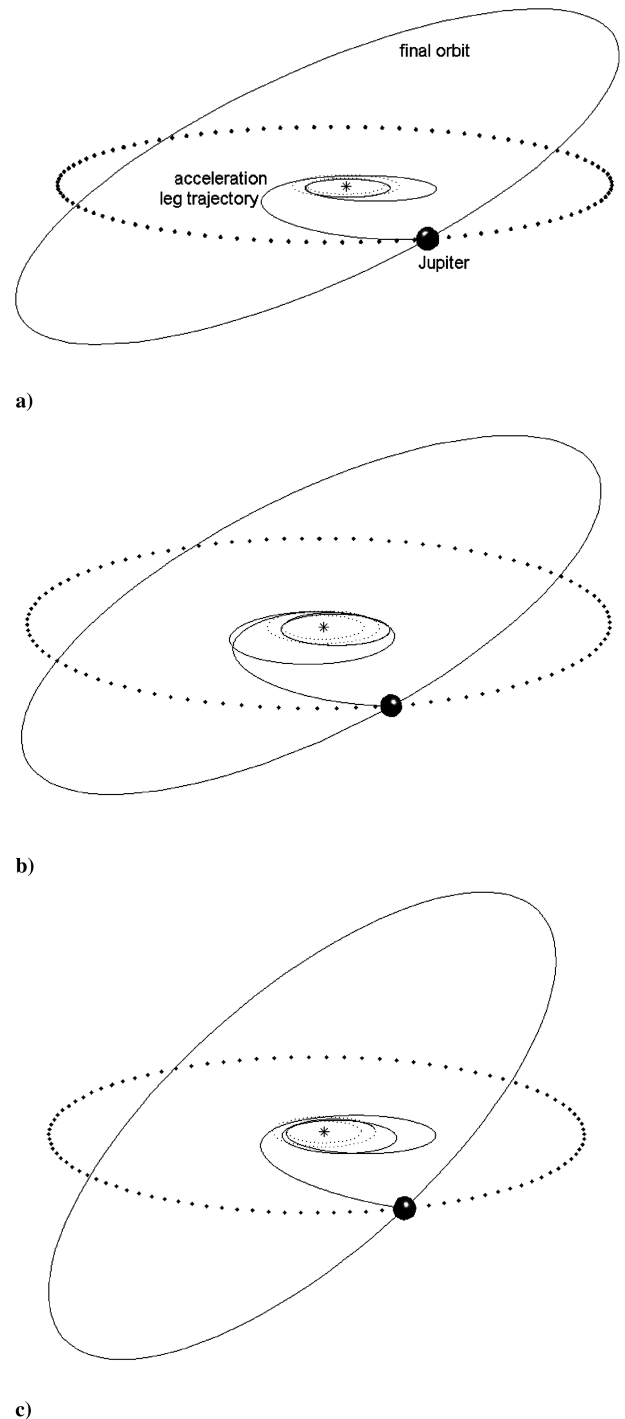


Fig. 8 Orbits for the final leg: a) EVEJ, b) EVVEJ, and c) EVVEJ.

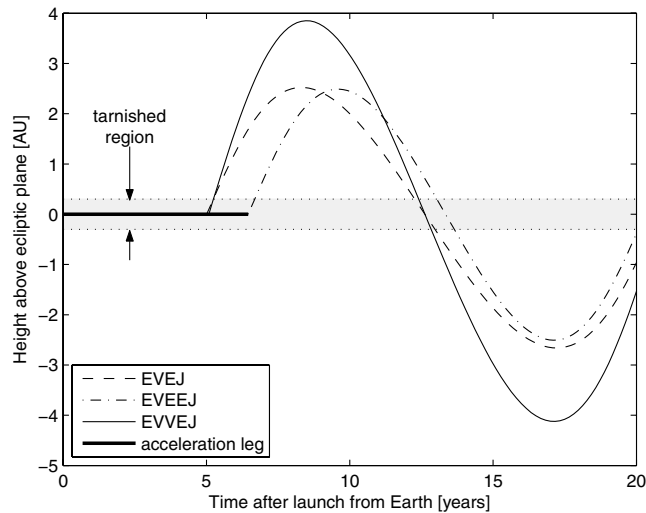


Fig. 9 Heights above the ecliptic as a function of the mission time for the EVEJ, EVEEJ, and EVVEJ trajectories.

Table 2 shows that the total observation times for the EVEJ, EVEEJ, and EVVEJ missions are, respectively, 14, 12.8, and 14.4 years. This renders the EVVEJ path best, as also pointed out in the previous section.

Table 1 shows that the acceleration leg times for EVEJ, EVEEJ, and EVVEJ transfers are roughly 5, 6.5, and 5 years, respectively. This leaves 15, 13.5, and 15 years, respectively, for the final-leg TOF. During the EVEEJ transfer, the spacecraft wastes much time, which cannot be compensated for during the final leg. Therefore, we are left with two preferable options: EVEJ and EVVEJ.

The final trajectory is produced to maximize t_{obs} (or minimize t_{tar}). In all cases (cf. Fig. 9), the spacecraft passes the tarnished region a minimal number of times (twice). The first time is when the spacecraft is rising up from the tarnished region, and the other time is when it is passing to the other side of the ecliptic plane. A large inclination of the final orbit enables the spacecraft to pass the tarnished region faster. A high $V_{\infty/J}$ results in a higher inclination of the final orbit. In the EVEJ case, $V_{\infty/J} = 6.21$ km/s, and for the EVVEJ case, $V_{\infty/J} = 9.14$ km/s (see Table 1). This is the reason for a higher t_{obs} in the EVVEJ case.

V. Conclusions

This paper considered orbit design for spaceborne observation missions. The goal was to develop highly inclined orbits to reduce sensitivity to the interplanetary dust noise. Suitable orbits were obtained by a gravity-assisted maneuver near Jupiter (J) when the spacecraft's hyperbolic excess velocity was high enough. Therefore, the first step of the orbit design was developing an Earth–Jupiter optimal multiple-gravity-assist trajectory through a series of planetary flybys near Earth (E) and Venus (V). The optimization was performed using a MA, which is based on the niching genetic algorithm. The travel paths of the selected trajectories were EVEJ, EVEEJ, and EVVEJ.

The second step was obtaining the highly inclined orbits after Jupiter flyby. The flybys were optimized to obtain final orbits with a long observation time. The resulting optimal observation times for EVEJ, EVEEJ, and EVVEJ are, respectively, 14, 12.8, and 14.4 years, during a 20-year mission lifetime. Because of the high Earth–Jupiter time of flight (6.5 years) and the low hyperbolic excess velocity relative to Jupiter (6.32 km/s), the EVEEJ trajectory can be excluded. Although its total impulse maneuver is relatively low (3.8 km/s), the time of flight is considerable. The EVEJ and EVVEJ

trajectories have relatively short Earth–Jupiter times of flight (5 years). The differences in the relative velocities near Jupiter (6.2 and 9.1 km/s for the EVEJ and EVVEJ transfers, respectively) did not result in a high difference in the observation times. Therefore, these two paths are the most suitable for spaceborne observation missions. Future research will examine the proposed orbits using a full-ephemeris simulation; in addition, optimal highly inclined trajectories will be found for much shorter mission lifetimes (5 years).

Acknowledgment

This work was partially supported by the Asher Space Research Institute of the Technion—Israel Institute of Technology.

References

- [1] "Terrestrial Planet Finder," California Inst. of Technology, Jet Propulsion Lab., Publ. 99-3, Pasadena, CA, May 1999.
- [2] Gurfil, P., Kasdin, N. J., Arrell, R., Seager, S., and Nissanke, S. M., "Infrared Space Observatories: How to Mitigate Zodiacal Dust Interference," *Astrophysical Journal*, Vol. 567, No. 2, Mar. 2002, pp. 1250–1261. doi:10.1086/338751
- [3] Gurfil, P., and Kasdin, N. J., "Optimal Out of Ecliptic Trajectories for Space-Borne Observatories," *Journal of the Astronautical Sciences*, Vol. 49, No. 4, 2001, pp. 509–537.
- [4] Szebeheley, V. G., *Theory of Orbits: The Restricted Problem of Three Bodies*, Academic Press, New York, 1967, pp. 117–130.
- [5] Strange, N. J., and Longuski, J. M., "Graphical Method for Gravity-Assist Trajectory Design," *Journal of Spacecraft and Rockets*, Vol. 39, No. 1, 2002, pp. 9–16. doi:10.2514/2.3800
- [6] Petropoulos, A. E., Longuski, J., and Bonfiglio, E. P., "Trajectories to Jupiter via Gravity Assists from Venus, Earth, and Mars," *Journal of Spacecraft and Rockets*, Vol. 37, No. 6, 2000, pp. 776–783. doi:10.2514/2.3650
- [7] Vasile, M., and De Pascale, P., "Preliminary Design of Multiple Gravity-Assist Trajectories," *Journal of Spacecraft and Rockets*, Vol. 43, No. 4, 2006, pp. 794–805. doi:10.2514/1.17413
- [8] Hartman, J. W., Coverstone-Carroll, V. L., and Williams, S. N., "Optimal Interplanetary Spacecraft Trajectories via a Pareto Genetic Algorithm," *Journal of the Astronautical Sciences*, Vol. 46, No. 3, July 1998, pp. 267–282.
- [9] Mahfoud, S. W., "Niching Methods for Genetic Algorithms," Univ. of Illinois at Urbana–Champaign, Illinois Genetic Algorithms Lab. Rept. 95001, Urbana, IL, 1995.
- [10] Knowles, J. D., and Corne, D. W., "M-PAES: A Memetic Algorithm for Multiobjective Optimization," *Proceedings of the 2000 IEEE Congress on Evolutionary Computation*, Inst. of Electrical and Electronics Engineers, Piscataway, NJ, 2000, pp. 325–332.
- [11] Goldberg, D. E., *Genetic Algorithms in Search, Optimization and Machine Learning*, Addison Wesley, Reading, MA, 1989, pp. 89–106.
- [12] Gurfil, P., and Kasdin, N. J., "Characterization and Design of Out of Ecliptic Trajectories Using Deterministic Crowding Genetic Algorithms," *Computer Methods in Applied Mechanics and Engineering*, Vol. 191, Nos. 19–20, 2002, pp. 2169–2186. doi:10.1016/S0045-7825(01)00380-2
- [13] Poincaré, H., *Les Méthodes Nouvelles de la Mécanique Céleste*, Vol. 3, Gauthier-Villars, Paris, 1899, pp. 362–371.
- [14] Pisarevsky, D. M., Kogan, A., and Guelman, M., "Building Interplanetary Trajectories with Multiple Gravity-Assisted Maneuvers," *Journal of Spacecraft and Rockets*, Vol. 44, No. 4, pp. 985–992. doi:10.2514/1.27888
- [15] Battin, R. H., *An Introduction to the Mathematics and Methods of Astrodynamics*, AIAA Education Series, AIAA, New York, 1987, pp. 295–313.

C. McLaughlin
Associate Editor